nature photonics

LETTERS

https://doi.org/10.1038/s41566-020-0657-2

Check for updates

# Phase-locked laser-wakefield electron acceleration

C. Caizergues[1]✉, S. Smartsev[1,2], V. Malka[1,2] and C. Thaury[1]

**Subluminal and superluminal light pulses have attracted considerable attention in recent decades[1–4], opening perspectives in telecommunications, optical storage and fundamental physics[5]. Usually achieved in matter, superluminal propagation has also been demonstrated in vacuum with quasi-Bessel beams[6,7] or spatio-temporal couplings[8,9]. Although, in the first case, the propagation was diffraction free, but with hardly controllable pulse velocities and limited to moderate intensities, in the second, high tunability was achieved, but with substantially lengthened pulse durations. Here we report a new concept that extends these approaches to relativistic intensities and ultrashort pulses by mixing spatio-temporal couplings and quasi-Bessel beams to independently control the light velocity and intensity. When used to drive a laser-plasma accelerator[10], this concept leads to a new regime that is dephasing free, where the electron beam energy gain increases by more than one order of magnitude.**

Electrical breakdown limits electric fields in radiofrequency accelerators to ~100 MeV m$^{-1}$. Laser-plasma accelerators (LPAs) commonly overcome this restriction by focusing ultrashort laser pulses in a gas to generate a co-travelling plasma wave[11] with accelerating fields (the wakefield) that are typically three orders of magnitude higher. These extreme fields allow for a drastic decrease in accelerator size for scientific, medical and industrial applications[12], making LPAs promising candidates for future high-energy colliders[13]. However, to reach high energies, an electron bunch trapped in the plasma wave has also to experience acceleration over long distances, which remains challenging in LPAs because of three phenomena: diffraction, pump depletion and dephasing[14]. Pump depletion (laser energy transfer to the plasma wave) and diffraction tend to decrease the laser intensity $I$ during its propagation to a level from which it can no longer drive a steady plasma wave ($I \lesssim 10^{18}$ W cm$^{-2}$). Dephasing originates from the difference between the electron bunch velocity and the laser velocity, which results in a progressive shift of the electrons towards a decelerating phase of the wakefield. Substantial research efforts have aimed to address these limitations[15–17]. Notably, a record energy of 8 GeV was obtained by guiding pulses in a capillary discharge[18], dealing with the limitations, but not removing them.

Here we propose an acceleration concept that allows us to simultaneously tackle these three phenomena, leading to new favourable energy scaling for LPAs. It uses high-intensity quasi-Bessel beams to generate the plasma wave and spatio-temporal couplings (STCs, dependencies in the laser field requiring a non-separable time–space description) to control its velocity. The quasi-Bessel beam is generated by focusing an ultrashort laser pulse with an axiparabola[19]. This aspheric mirror produces a long focal line by reflecting rays towards different focal positions $f$ according to their impinging coordinate on the mirror surface, according to $f(r)=f_0+\delta(r)$, where $f_0$ is the small radius focus and $\delta$ is a function determining the intensity distribution. This optics is similar to axilenses[20], but, in contrast to such refractive counterparts, the axiparabola can focus the laser with a high enough intensity to drive a steady plasma wave[19], leading to a propagation regime that it has not been possible to achieve with Bessel beams[21,22]. Diffraction is naturally addressed, because the focal line can be much larger than the Rayleigh length of a Gaussian beam of the same numerical aperture. The accelerator is also free of pump depletion, because the plasma wave is excited by fresh rays originating from different $r$ at each position along the focal line $z=f(r)$. In other words, the effective diffraction and depletion lengths equal the focal depth of the axiparabola by construction. Dephasing thus remains the only limit requiring fixing, which implies controlling the laser velocity.

The velocity of the axial intensity peak in vacuum (also its phase velocity, in this case) is $v_z=\mathrm{d}f/\mathrm{d}t$, where $t(r)$ is the focusing time, thus giving, in the ray optics approximation (see Supplementary Information):

$$\frac{v_z}{c} = 1 + \frac{r^2}{2f^2} \tag{1}$$

Equation (1) shows that $v_z(z)$ is superluminal, with variations along the optical axis imposed by the choice of $\delta(r)$. However, STCs bring additional degrees of freedom. In particular, a radially dependent pulse front delay $\Delta_t(r)$ leads to a modified focusing time $t+\Delta_t$ but unchanged focusing position, hence tailoring $v_z$. Within a plasma (of electron density $n_e$), the pulse velocity shifts in the paraxial approximation by $\Delta v_z=v_g-c$, where $v_g$ is the group velocity in the plasma. In the context of LPAs, the delay should be chosen to match the velocities of the pulse and of the electron beam ($\sim c$), hence suppressing dephasing. STCs have thus to compensate for both $\Delta v_z$ and the velocity change in equation (1), leading to

$$c - \Delta v_z = \frac{\partial_r f}{\partial_r (t + \Delta_t)} \tag{2}$$

The principle of this phase-locked acceleration is illustrated in Fig. 1 (lower part). Appropriate STCs could be applied by using a spatial light modulator and deformable mirrors[23], or chromatic optics[24], for example. Figure 2 compares, for a constant-intensity focal line (see Supplementary Information), the maximum peak intensity and velocity evolution with and without STCs, stemming from linear spectral propagation simulations[25] in vacuum. As expected, a constant-intensity line is actually obtained in both cases (Fig. 2a), while application of the appropriate $\Delta_t$ for a homogeneous plasma (Fig. 2c) leads, in vacuum, to a constant superluminal ($c-\Delta v_z$) velocity (Fig. 2b).

Once diffraction, pump depletion and dephasing are overcome, the only limit to the electron beam energy gain $\Delta W$ is the achievable accelerating field, $E_z$, along the focal line. The maximum field

[1]Laboratoire d'Optique Appliquée, Ecole polytechnique – ENSTA – CNRS – Institut Polytechnique de Paris, Palaiseau, France. [2]Department of Physics of Complex Systems, Weizmann Institute of Science, Rehovot, Israel. ✉e-mail: clement.caizergues@ensta-paristech.fr

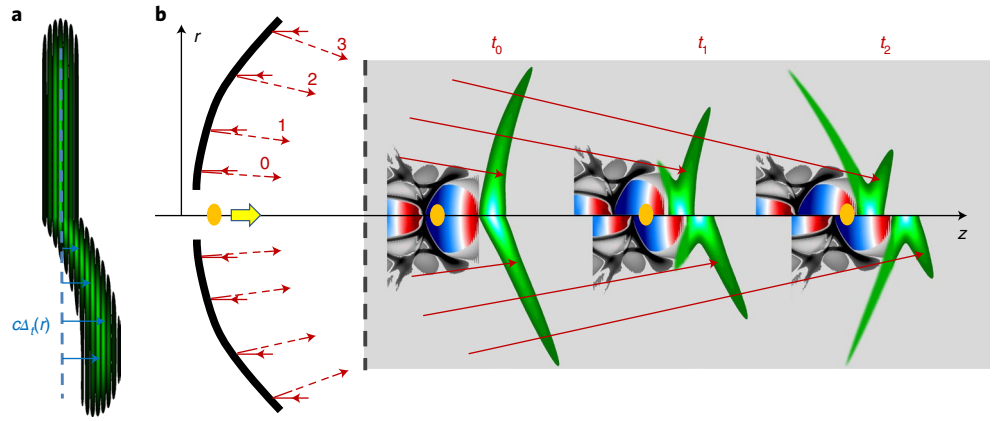


**Fig. 1 | Schematic view of laser-plasma acceleration with an axiparabola, without and with STCs.** The top half shows a schematic wihout STCs, and the bottom half a schematic with STCs added as a radially dependent pulse front delay $\Delta_i(r)$ to lead to phase-locked acceleration. **a**, The laser pulse at the axiparabola. **b**, Evolution along the focal line of the laser pulse (dark green to light blue colour scale) and its co-travelling electron plasma wave (grey levels) sustaining strong wakefields (blue to red). Three propagation times are illustrated (ray *i* focuses at $t_i$). With STCs, an externally launched relativistic electron bunch (orange dot) remains in phase with the strongest accelerating wakefield (dark blue), whereas it slips towards a decelerating region (red) in the case without STCs.

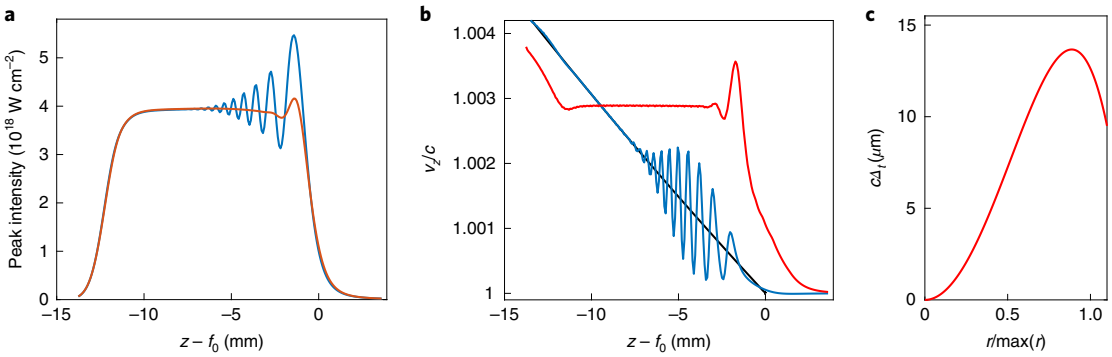


**Fig. 2 | Comparison, for a constant-intensity focal line, of the maximum peak intensity and velocity evolution with and without STCs, stemming from linear spectral propagation simulations in vacuum. a–c**, Maximum intensity (**a**) and peak velocity (**b**) along a 12 mm focal line obtained by focusing a 1 J, 15 fs top-hat laser pulse in vacuum with an *f*/6 axiparabola. Blue curves correspond to the case without STCs and red curves to the case with the pulse front delay displayed in **c**. The black curve in **b** shows the prediction from equation (1). An 800 nm central wavelength and a plasma density of $1.0\times10^{19}$ cm$^{-3}$ were assumed for calculation of the STCs, which were applied at the axiparabola position (see Supplementary Information). Oscillations arise from interference effects, beyond the ray approximation description. STCs appear to smooth these effects.

amplitude in LPAs verifies $E_z \propto \sqrt{n_e}$, where the proportionality factor depends both on the laser pulse shape and normalized vector potential $a_0 = eA/(m_e c^2)$ (ref. [14]). In regular LPAs[10], maintaining high fields requires the plasma wave to be resonantly excited, which constrains the choice of laser duration $\tau$ and spot size $w_0$ towards $c\tau \approx w_0 \approx \lambda_p$, where $\lambda_p \propto 1/\sqrt{n_e}$ is the plasma wavelength. Here, thanks to diffraction-free focusing, the choice of $w_0$ does not affect the propagation length, so the resonance condition mainly reduces to $c\tau \approx \lambda_p$. Moreover, the focal depth (and so the acceleration length) can be set to be arbitrarily long, but the longer the focal depth, the lower the intensity. For a top-hat beam and a constant-intensity focal line of length $\delta_0$, the normalized vector potential is given by (see Supplementary Information)

$$a_0 \approx 0.68\sqrt{\lambda_0 P_0/\delta_0} \tag{3}$$

where $\lambda_0$ is the laser central wavelength (in μm), $P_0$ is the incident power (in TW) and $\delta_0$ is in units of mm. The choice of $a_0$ determines the interaction regime; higher $a_0$ leads to stronger $E_z$, but also to stronger nonlinear propagation effects, altering the wakefield stability. In the following, we assumed $a_0 \approx 1.5$, which appeared to be a good trade-off. As setting $a_0$ fixes the ratio $P_0/\delta_0$ in equation (3), the energy gain for a phase-locked acceleration with a resonant pulse duration is

$$\Delta W = -eE_z\delta_0 \propto P_0\sqrt{n_e} \tag{4}$$

$$\propto W_L/\tau^2 \tag{5}$$

where $W_L$ is the laser energy. To determine the relation between $E_z$ and $\sqrt{n_e}$ involved in equation (5), particle-in-cell (PIC) simulations were carried out, varying $n_e$, $\tau$ and the axiparabola parameters (see Methods and Supplementary Information). Figure 3 reports the evolution of energy gain (stemming from equation (5)) with laser energy and duration. Two new trends emerge: (1) gain proportional to the laser energy and acceleration length and (2) drastically increased gains towards shorter laser pulses and denser plasmas. Conversely,

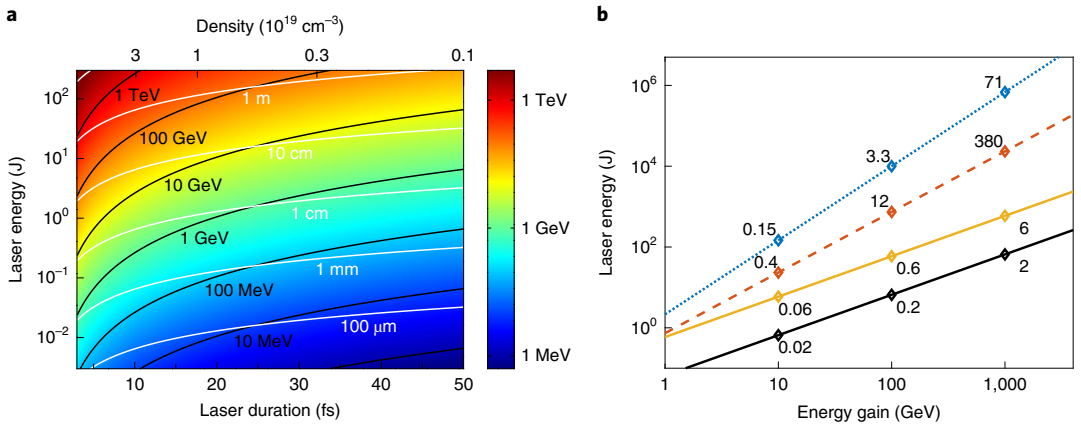


**Fig. 3 | Evolution of energy gain with accelerator, laser and plasma parameters. a**, Maximal energy gain from phase-locked LPAs (colourmap) as a function of laser energy and duration. Lines indicate the evolution for a few energy gains (black) and a few acceleration lengths (white). The upper *x* axis specifies the corresponding electron density. **b**, Laser energy scaling with energy gain, from standard self-guided LPAs (blue dotted line), externally guided LPAs (red dashed line) and from phase-locked LPAs (solid curves) with 15 fs (yellow) and 5 fs (black) laser durations. Diamonds indicate some corresponding acceleration lengths (in m). Condition $c\tau = \lambda_p/2$ was assumed for phase-locked acceleration.

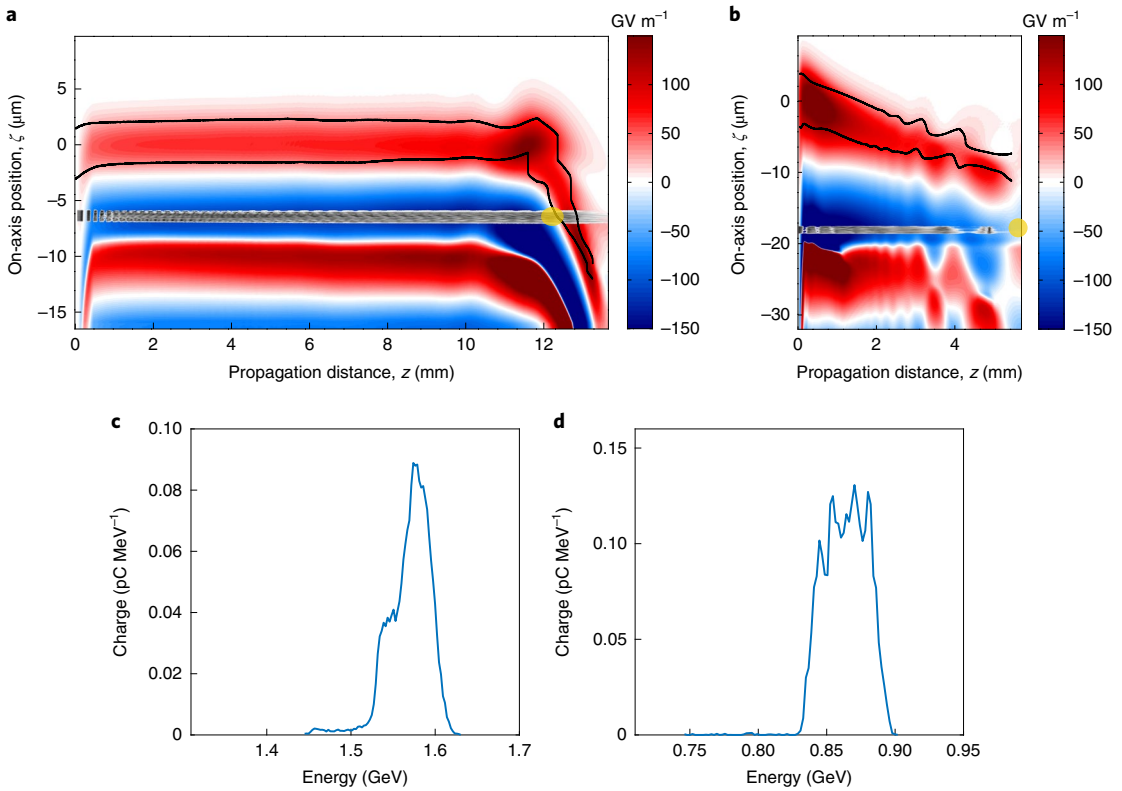


**Fig. 4 | PIC simulations of phase-locked acceleration and standard LPA, with an externally injected electron bunch and the same laser energy. a**,**b**, In a *c*-travelling window, evolution of the on-axis accelerating field $E_z$ (blue to red colourmap) of the electron bunch density (grey arbitrary unit) and of the laser half-maxima (black lines) along propagation for phase-locked acceleration (**a**) and standard LPA (**b**). The pulse maximum at its entrance in the plasma is located at $\zeta = 0$ µm. Yellow dots mark the end of the acceleration. **c**,**d**, Electron energy spectrum at the acceleration end from phase-locked acceleration (**c**) and standard LPA (**d**).

dephasing limitations push regular high-energy LPAs towards longer and more energetic pulses propagating in low-density plasmas and over long acceleration lengths[14]. For example, ref. [10] estimated a gain $\Delta W = 120$ GeV from a 1,120 J laser propagating in an 18 m plasma channel of minimum density $n_e = 1.0 \times 10^{16}$ cm$^{-3}$. For the same energy gain, Fig. 3a indicates that 71 J are required for a 15 fs laser, and only 20 J for an 8 fs duration, that is, almost two orders of magnitude less. Importantly, the propagation is also drastically shortened to a few tens of centimetres (Fig. 3b) and does not require any guiding. The flying focus technique[8,9], relying on STCs and spectral chirp, allows for similar tailored velocities and extended Rayleigh lengths, but the large chromatic dispersion required to

produce the extended Rayleigh lengths results in increased pulse duration. This prevents its application to phase-locked acceleration, which requires both short pulses and long acceleration distances.

To confirm these estimates, we performed PIC simulations (see Methods). Owing to the high phase velocity, trapping electrons in the wakefield require external injection or controlled injection schemes, such as density transition[26] and/or colliding-pulse injection[27]. For the sake of simplicity, we consider only the case of a 200 MeV externally injected electron bunch. Figure 4a,b reports the on-axis evolution of the wakefield in a $c$-travelling window (axial coordinate $\zeta = z - ct$). The initial settings of Fig. 2 were used for the simulation plotted in Fig. 4a,c. As expected from optimal phase-locking, the electron beam (located at $\zeta \approx -6\,\mu m$) remains in an accelerating phase until the end of the focal line ($z \approx 12\,mm$), where fresh rays no longer arrive and the central part of the pulse self-focuses. For the same laser energy, Fig. 4b illustrates the standard acceleration from a Gaussian pulse with propagation parameters maximizing $\Delta W$ (ref. [10]). Here, the electron beam progressively dephases, ending the acceleration at $z \approx 6\,mm$. The bunch spectra show respective gains of 1.4 GeV (Fig. 4c) and 0.65 GeV (Fig. 4d), in good agreement with predictions. As expected for $a_0 \approx 1.5$, deviations from theoretical modelling appear very limited in Fig. 4a, restraining nonlinear propagation effects to the axis vicinity. Indeed, before attaining $z = f(r)$, beamlets originating from on-mirror radius $r$ travel at low intensities, enabling an almost linear propagation. With gas targets, such low-intensity beamlets may require a preexisting plasma to avoid experiencing defocusing gradients from ionization fronts. Focusing the outer rays first ($\delta(r) < 0$) should limit this requirement, avoiding the propagation of large-aperture, low-intensity beamlets on many Rayleigh lengths and also minimizing the target volume to be ionized.

In conclusion, the proposed concept sets us free from the three phenomena that limit acceleration in LPAs. This phase-locked LPA (along with ongoing advances in laser technology) opens unique opportunities. Coupled with high-repetition-rate few-cycle lasers[28,29], it will boost the development of compact, flexible and bright particle and radiation sources for applications[12]. For example, 1 GeV electron beams could be generated, at a 1 kHz repetition rate, from a 12 TW, 5 fs laser pulse. When used with multi-petawatt lasers[30], phase-locked LPAs offer the possibility to drastically reduce both the acceleration length and the required pulse energy (and thus the set-up complexity and facility cost), which could be decisive in the design of plasma-based colliders. For example, a single acceleration stage of 6 m, driven by a 37 PW, 15 fs laser pulse, could produce electron beams of up to 1 TeV. Propagating a few-femtosecond pulse over long lengths should, however, be affected by dispersion-broadening. This could be mitigated by limiting the pulse front delay, for example by using a discontinuous mirror surface to allow for quasi-phase-locking or by designing a mirror that optimizes the radial delay and by jointly shaping the radial laser intensity profile to keep a constant $a_0$ along $z$. Propagation would also benefit from tailored plasma geometries aiming to reduce the crossed length of plasma, as well as from chirped-pulse or advanced STCs. Finally, density variations along $z$ could allow us to balance the pulse lengthening through better plasma wave coupling. In parallel, high-energy positron beams could be produced with the same scheme by using laser pulses carrying orbital momentum to generate hollow focal lines[31]. The versatility of the proposed concept, which enables both laser diffraction and velocity control (with possibly complex evolution), should also benefit other plasma-based particle and radiation sources, such as free-electron lasers, X-ray lasers[32], Compton scattering[33] and betatron[34] sources, as well as frequency converters[35]. Similar to Bessel beams[36], it could also be used for high-order harmonic generation, with the advantage that the pulse front delay uncouples the group velocity from the laser phase velocity.

## Online content

Any methods, additional references, Nature Research reporting summaries, source data, extended data, supplementary information, acknowledgements, peer review information; details of author contributions and competing interests; and statements of data and code availability are available at https://doi.org/10.1038/s41566-020-0657-2.

Received: 18 February 2019; Accepted: 3 June 2020;
Published online: 6 July 2020

## References

1. Wang, L. J., Kuzmich, A. & Dogariu, A. Gain-assisted superluminal light propagation. *Nature* **406**, 277–279 (2000).
2. Bigelow, M. S., Lepeshkin, N. N. & Boyd, R. W. Superluminal and slow light propagation in a room-temperature solid. *Science* **301**, 200–203 (2003).
3. Stenner, M. D., Gauthier, D. J. & Neifeld, M. A. The speed of information in a 'fast-light' optical medium. *Nature* **425**, 695–698 (2003).
4. Thévenaz, L. Slow and fast light in optical fibres. *Nat. Photon.* **2**, 474–481 (2008).
5. Boyd, R. Slow and fast light: fundamentals and applications. *J. Mod. Opt.* **56**, 1908–1915 (2009).
6. Alexeev, I., Kim, K. Y. & Milchberg, H. M. Measurement of the superluminal group velocity of an ultrashort Bessel beam pulse. *Phys. Rev. Lett.* **88**, 073901 (2002).
7. Mugnai, D., Ranfagni, A. & Ruggeri, R. Observation of superluminal behaviors in wave propagation. *Phys. Rev. Lett.* **84**, 4830–4833 (2000).
8. Sainte-Marie, A., Gobert, O. & Quéré, F. Controlling the velocity of ultrashort light pulses in vacuum through spatio-temporal couplings. *Optica* **4**, 1298–1304 (2017).
9. Froula, D. H. et al. Spatiotemporal control of laser intensity. *Nat. Photon.* **12**, 262–265 (2018).
10. Lu, W. et al. Generating multi-GeV electron bunches using single stage laser wakefield acceleration in a 3D nonlinear regime. *Phys. Rev. ST Accel. Beams* **10**, 061301 (2007).
11. Tajima, T. & Dawson, J. M. Laser electron accelerator. *Phys. Rev. Lett.* **43**, 267–270 (1979).
12. Malka, V. et al. Principles and applications of compact laser plasma accelerators. *Nat. Phys.* **4**, 447–453 (2008).
13. Schroeder, C. B., Esarey, E., Geddes, C. G. R., Benedetti, C. & Leemans, W. P. Physics considerations for laser-plasma linear colliders. *Phys. Rev. ST Accel. Beams* **13**, 101301 (2010).
14. Esarey, E., Schroeder, C. B. & Leemans, W. P. Physics of laser-driven plasma-based electron accelerators. *Rev. Mod. Phys.* **81**, 1229–1285 (2009).
15. Steinke, S. et al. Multistage coupling of independent laser-plasma accelerators. *Nature* **530**, 190–193 (2016).
16. Leemans, W. P. et al. GeV electron beams from a centimetre-scale accelerator. *Nat. Phys.* **2**, 696–699 (2006).
17. Guillaume, E. et al. Electron rephasing in a laser-wakefield accelerator. *Phys. Rev. Lett.* **115**, 155002 (2015).
18. Gonsalves, A. J. et al. Petawatt laser guiding and electron beam acceleration to 8 GeV in a laser-heated capillary discharge waveguide. *Phys. Rev. Lett.* **122**, 084801 (2019).
19. Smartsev, S. et al. Axiparabola: a long-focal-depth, high-resolution mirror for broadband high-intensity lasers. *Opt. Lett.* **44**, 3414–3417 (2019).
20. Davidson, N., Friesem, A. A. & Hasman, E. Holographic axilens: high resolution and long focal depth. *Opt. Lett.* **16**, 523–525 (1991).
21. Hafizi, B., Esarey, E. & Sprangle, P. Laser-driven acceleration with Bessel beams. *Phys. Rev. E* **55**, 3539–3545 (1997).
22. Kumar, S., Parola, A., Di Trapani, P. & Jedrkiewicz, O. Laser plasma wakefield acceleration gain enhancement by means of accelerating Bessel pulses. *Appl. Phys. B* **123**, 185 (2017).
23. Sun, B., Salter, P. S. & Booth, M. J. Pulse front adaptive optics: a new method for control of ultrashort laser pulses. *Opt. Express* **23**, 19348–19357 (2015).
24. Cui, Z. et al. Dynamic chromatic aberration pre-compensation scheme for ultrashort petawatt laser systems. *Opt. Express* **27**, 16812–16822 (2019).
25. Guizar-Sicairos, M. & Gutiérrez-Vega, J. C. Computation of quasi-discrete Hankel transforms of integer order for propagating optical wave fields. *J. Opt. Soc. Am. A* **21**, 53–58 (2004).
26. Schmid, K. et al. Density-transition based electron injector for laser driven wakefield accelerators. *Phys. Rev. ST Accel. Beams* **13**, 091301 (2010).
27. Faure, J. et al. Controlled injection and acceleration of electrons in plasma wakefields by colliding laser pulses. *Nature* **444**, 737–739 (2006).
28. Budriūnas, R. et al. 53-W average power CEP-stabilized OPCPA system delivering 5.5-TW few cycle pulses at 1-kHz repetition rate. *Opt. Express* **25**, 5797–5806 (2017).
29. Rivas, D. E. et al. Next generation driver for attosecond and laser-plasma physics. *Sci. Rep.* **7**, 5224 (2017).

30. Cartlidge, E. The light fantastic. *Science* **359**, 382–385 (2018).
31. Vieira, J. & Mendonça, J. T. Nonlinear laser driven donut wakefields for positron and electron acceleration. *Phys. Rev. Lett.* **112**, 215001 (2014).
32. Depresseux, A. et al. Table-top femtosecond soft X-ray laser by collisional ionization gating. *Nat. Photon.* **9**, 817–821 (2015).
33. Phuoc, K. T. et al. All-optical Compton gamma-ray source. *Nat. Photon.* **6**, 308–311 (2012).
34. Corde, S. et al. Femtosecond X-rays from laser-plasma accelerators. *Rev. Mod. Phys.* **85**, 1–48 (2013).
35. Nie, Z. et al. Relativistic single-cycle tunable infrared pulses generated from a tailored plasma density structure. *Nat. Photon.* **12**, 489–494 (2018).
36. Averchi, A. et al. Phase matching with pulsed Bessel beams for high-order harmonic generation. *Phys. Rev. A* **77**, 021802 (2008).

## Methods

**PIC simulations.** PIC simulations were performed with the three-dimensional PIC code CALDER-Circ[37], which relies on a cylindrical mesh ($r$,$z$) and a Fourier decomposition in the poloidal direction to take advantage of the laser symmetries and reduce the computational time. The simulation in Fig. 4a,c was performed with mesh sizes of $\mathrm{d}r = 0.8k^{-1}$ and $\mathrm{d}z = 0.2k^{-1}$ (where $k$ is the wavenumber at 800 nm) and the two first Fourier modes. The plasma (of density $1.0\times10^{19}\,\mathrm{cm}^{-3}$) started with a 500-μm linear ramp and was initially neutral with a fixed ion background. The number of electrons per cell was 100 close to the optical axis and reduced to 10 for $r > 15\,\mu\mathrm{m}$. The beginning of the plasma ramp and the beginning of the focal line ($z = f_0 - \delta_0$) were matched. The profile of the on-axis injected electron bunch was assumed trapezoidal, with $7k^{-1}$ axial and $6k^{-1}$ radial plateaux (at density $1.25\times10^{19}\,\mathrm{cm}^{-3}$, leading to 4.5 pC charge) and $1k^{-1}$ ramps in each direction, and initial thermal effects were neglected. For finite mesh sizes, PIC calculations introduce numerical dispersion and thus a non-physical offset in the laser pulse velocity $\Delta v_{\mathrm{num}}$. With previous parameters, this effect would prevent phase-locked acceleration on the whole focal line. Finer meshes would reduce this deleterious contribution, but at the price of a substantial increase in the simulation cost (evolution as $1/\mathrm{d}z^2\mathrm{d}r$), beyond our computational resources at the time of this study. Rather, we chose to fully precompensate for this velocity shift by replacing $c - \Delta v_z$ by $c - \Delta v_z - \Delta v_{\mathrm{num}}$ in equation (2). Figure 4b mesh parameters were $\mathrm{d}r = 1.2k^{-1}$ and $\mathrm{d}z = 0.1k^{-1}$. The up ramp was 100-μm-long and the 25 fs Gaussian pulse was focused to an 11-μm spot size at the end of the ramp, then propagated in a plasma with density of $3.2\times10^{18}\,\mathrm{cm}^{-3}$. The externally injected bunch had the same spatial features as for the phase-locked simulation, with a 5 pC charge.

**Estimation of the accelerating field.** Several PIC simulations were carried out to determine the relation between the accelerating wakefield and the plasma density while using axiparabolas. Different top-hat pulses at 800 nm were focused by different axiparabolas (not necessary in a phase-locked configuration) and we averaged along the focal line the maximal accelerating field along the propagation. That led to the estimation $E_z(\,\mathrm{GV\,m^{-1}}) \approx 76a_0^{1.5}\sqrt{n_{\mathrm{e}}(10^{19}\,\mathrm{cm}^{-3})}$ (see Supplementary Information), that is $E_z(mc\omega_{\mathrm{p}}/e) \approx 0.25a_0^{1.5}$, in normalized units.

## Data availability

The data that support the plots and findings of this paper are available from the corresponding author upon reasonable request.

## References

37. Lifschitz, A. et al. Particle-in-cell modelling of laser-plasma interaction using Fourier decomposition. *J. Comput. Phys.* **228**, 1803–1814 (2009).

## Acknowledgements

We acknowledge support from the European Research Council through the project XFive (grant no. 339128), the French Agence Nationale de la Recherche (ANR) under reference ANR-19-TERC-0001-01 (project TGV), Gerry Schwartz and Heather Reisman, Israel Science Foundation, VATAT support and the French embassy in Israel through a Chateaubriand fellowship.

## Author contributions

C.C. and C.T. jointly proposed the concept of phase-locked acceleration, using axiparabola and spatio-temporal couplings. The idea was then developed by C.C. with advice from V.M. and C.T. C.C. and C.T. established the theoretical background, while C.C. and S.S. developed codes for optimizing and simulating axiparabola focus. Simulations were carried out by C.C. Finally, C.C. and C.T. wrote the manuscript with help from V.M. and S.S.

## Competing interests

C.T. and S.S. have filed a patent application (no. EP18305810.6) on axiparabola. The authors declare no other competing interests.

## Additional information

**Supplementary information** is available for this paper at https://doi.org/10.1038/s41566-020-0657-2.

**Correspondence and requests for materials** should be addressed to C.C.

**Reprints and permissions information** is available at www.nature.com/reprints.